

High-efficiency reflection phase tunable metasurface atnear-infrared frequencies

Ce Li(李策), Wei Zhu(朱维), Shuo Du(杜硕), Junjie Li(李俊杰), Changzhi Gu(顾长志)

Citation: Chin. Phys. B, 2021, 30 (**5**): 057802. DOI: 10.1088/1674-1056/abe9a6
Journal homepage: http://cpb.iphy.ac.cn; http://iopscience.iop.org/cpb

What follows is a list of articles you may be interested in

Absorption interferometer of two-sided cavity

Miao-Di Guo(郭苗迪), Hong-Mei Lii(李红梅)
Chin. Phys. B, 2021, 30 (**5**): 054202. DOI: 10.1088/1674-1056/abdea4

Dual-function beam splitter of high contrast gratings

Wen-Jing Fang(房文敬), Xin-Ye Fan(范鑫烨), Hui-Juan Niu(牛慧娟), Xia Zhang (张霞), Heng-Ying Xu(许恒迎), and Cheng-Lin Bai(白成林)
Chin. Phys. B, 2021, 30 (**4**): 044205. DOI: 10.1088/1674-1056/abd68d

Controlling the light wavefront through a scattering medium based on direct digital frequency synthesis technology

Yuan Yuan(袁园), Min-Yuan Sun(孙敏远), Yong Bi(毕勇), Wei-Nan Gao(高伟男), Shuo Zhang(张硕), and Wen-Ping Zhang(张文平)
Chin. Phys. B, 2021, 30 (**1**): 014209. DOI: 10.1088/1674-1056/abb665

Active metasurfaces for manipulatable terahertz technology

Jing-Yuan Wu(吴静远), Xiao-Feng Xu(徐晓峰), Lian-Fu Wei(韦联福)
Chin. Phys. B, 2020, 29 (**9**): 094202. DOI: 10.1088/1674-1056/aba613

Polarization readout analysis for multilevel phase change recording by crystallization degree modulation

Lin Jin-Cheng, Long Guo-Yun, Wang Yang, Wu Yi-Qun
Chin. Phys. B, 2013, 22 (**12**): 124208. DOI: 10.1088/1674-1056/22/12/124208

High-efficiency reflection phase tunable metasurface at near-infrared frequencies*

Ce Li(李策)[1,2], Wei Zhu(朱维)[3], Shuo Du(杜硕)[1,2], Junjie Li(李俊杰)[1,2,4], and Changzhi Gu(顾长志)[1,2,5,†]

[1] *Beijing National Laboratory for Condensed Matter Physics, Institute of Physics, Chinese Academy of Sciences, Beijing* 100190, *China*
[2] *School of Physical Sciences, CAS Key Laboratory of Vacuum Physics, University of Chinese Academy of Sciences, Beijing* 100049, *China*
[3] *Key Laboratory of Space Applied Physics and Chemistry, Ministry of Education and Department of Applied Physics, School of Science, Northwestern Polytechnical University, Xi'an* 710129, *China*
[4] *Songshan Lake Materials Laboratory, Dongguan* 523808, *China*
[5] *Collaborative Innovation Center of Quantum Matter, Beijing* 100871, *China*

(Received 14 January 2021; revised manuscript received 22 February 2021; accepted manuscript online 25 February 2021)

The realization of active modulation of reflection phase based on metasurfaces is of great significance for flexible control of electromagnetic wavefront, which makes metasurfaces have practical application values in polarization conversion, beam steering, metalens, etc. In this paper, a reflection phase tunable gap-surface plasmon (GSP) metasurface based on phase change materials $Ge_2Sb_2Te_5$ (GST) is designed and experimentally demonstrated. By virtue of the characteristics of large permittivities difference before and after GST phase transition and the existence of stable intermediate states, the continuous modulation of near-infrared reflection phase larger than 200° has been realized. At the same time, through the reasonable design of the structure sizes, the reflection has been maintained at about 0.4 and basically does not change with the GST phase transition, which improved the working efficiency of the metasurface significantly. In addition, the coupled-mode theory (CMT) is introduced to make a full analysis of the modulation mechanism of the reflection phase, which proves that the phase transition of GST can induce the transition of metasurface working state from overcoupling mode to critical coupling mode. The improvement of the metasurface working efficiency has practical values for wavefront modulation.

Keywords: active metasurface, phase change materials, phase modulation

PACS: 42.79.−e, 42.79.Fm, 78.67.Pt **DOI:** 10.1088/1674-1056/abe9a6

1. Introduction

Metasurfaces are artificially constructed arrays of nanostructured elements with subwavelength thickness arranged in a periodic or quasi-periodic form.[1,2] Due to their unique characteristics of low dimension, simple fabrication methods, and easy on-chip integration, metasurfaces have been widely used in many fields since they were proposed.[3] Metasurfaces can not only effectively control the amplitude of the electromagnetic wave to realize perfect absorption, but also precisely manipulate the phase of electromagnetic waves, so that they have new application values in beam steering,[4–6] electromagnetic lens,[7–10] holographic imaging,[11–14] etc.

As a specific branch of plasmonic metasurfaces, gap-surface plasmon (GSP) metasurfaces,[15] which consist of a subwavelength thin dielectric spacer sandwiched between an optically thick metal film and arrays of metal subwavelength nanostructures, can make the reflection phase of the electromagnetic wave changes a full 360° range,[16] greatly improving the phase control ability of the metasurfaces and providing a foundation for the application of functional metadevices based on phase manipulation. With the combination of GSP metasurfaces of geometric phase,[5,17] 360° gradient change of reflected phase at the same frequency can be realized through the method of rotating the metasurface element structure. However, this method is only applicable to circularly polarized incident light thus has great limitations in applications. For the case of the linearly polarized incident wave, there are mainly two different methods to control the reflection phase with the help of GSP metasurfaces. First, the shape and size of the top metal structures are designed and optimized with the dielectric spacer and metal film remain unchanged, so as to realize the gradient change of reflection phase of 360°. For example, in 2013, Bozhevolnyi *et al.* proposed that meta nanobrick and nanocross elements could change the reflected phase within 360° of the incident linear polarization of TM and TE simultaneously through size optimization and combination, thus obtaining the metasurface with abnormal reflection function.[6] However, this method has rigorous requirements on the sizes of metal structures, which brings difficulties to the design and experiment. Furthermore, the designed devices have relatively single functions. The other method

*Project supported by the National Key Research and Development Program of China (Grant Nos. 2016YFA0200400, 2016YFA0200800, and 2016YFA0300601), the National Natural Science Foundation of China (Grant Nos. 61888102,11674387, 11974386, and 61905274), the Strategic Priority Research Program and Key Research Program of Frontier Sciences of Chinese Academy of Sciences (Grant Nos. XDB33000000, XDB28000000, and QYZDJ-SSW-SLH042).

†Corresponding author. E-mail: czgu@iphy.ac.cn

© 2021 Chinese Physical Society and IOP Publishing Ltd

is to change the reflection phase by active modulation.[18–22] For example, Park *et al.* proposed in 2016 that by modulating the carrier concentrations of ITO dielectric layer with bias voltage, GSP metasurfaces with Au nanostripesarray top structures can achieve the modulation effects with reflective phase over 180°.[18] In 2018, Atwater *et al.* further increased the freedom of active modulation by introducing the dual-gate method and improved the regulation of reflected phase angle to more than 300°, further satisfying the practical needs.[19] The approach based on active modulation to realize reflection phase tuning, which is no longer dependent on complex structural design, has higher flexibility and provides the possibility to realize multi-function device integration.[20]

The existing reflection phase control based on metasurface active modulation has extended the control range by more than 180°, but it usually comes at the expense of the reflection, and at the same time, the reflection changes obviously with the phase modulation, making the work of the metasurfaces inefficient. To solve these problems, in this paper, an active GSP metasurface based on phase change material $Ge_2Sb_2Te_5$ (GST) has been proposed. By using the characteristics of large discrepancies of permittivities before and after the phase transition and stable intermediate states of GST,[23,24] the wide and continuous reflection phase modulation in the near-infrared has been achieved. At the same time, high and stable reflection is guaranteed by precious control of the structure sizes. In addition, the coupled-mode theory (CMT)[25,26] has been introduced to make full explanations on these modulation effects.

2. Results and discussion

The schematic of the reflection phase tunable GSP metasurface is shown in Fig. 1(a). The total structure employed in this work has a typical metal-dielectric-metal configuration which consists of an Au grating array stacked above a 20 nm thick SiO_2 protective layer and a 60 nm GST active dielectric layer and 100-nm-thick bottom Au mirror layer. The Au grating structure has a period of $p = 360$ nm with width $w = 120$ nm and thickness $t = 50$ nm.

The designed metasurface was implemented by nanofabrication. To begin with, a 100-nm-thick Au film and a 60-nm-thick GST film were deposited successively on Si substrate by direct current (DC) and radio frequency (RF) magnetron sputtering (MS) methods. The deposition of GST was performed from a synthesized single target with the growth pressure at 1 mTorr by a throttle valve with the argon (Ar) gas flow rate of 10 sccm and growth power at 100 W. Both the Au film and the GST film were grown at room temperature, and thus the resulting GST exhibited an amorphous state. Then a 20 nm SiO_2 layer was deposited as the protective layer using a plasma-enhanced chemical vapor deposition (PECVD) system. To avoid the phase change of GST caused by regular high growth temperature, the deposition temperature was controlled at 110°. The pattern of grating structures was obtained by the electron-beam lithography (EBL) technique. After development, 3 nm Cr and 50 nm Au film were deposited using electron-beam evaporation (EBE), followed by a lift-off procedure in 60° acetone. The total array size is 120 μm×120 μm. Figure 1(b) shows the scanning electron microscope (SEM) image of the fabricated metasurface for amorphous GST.

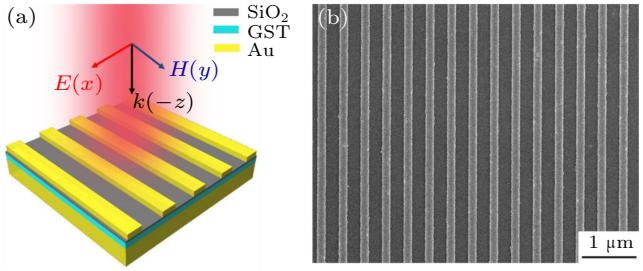


Fig. 1. (a) Schematic of the reflection phase tunable GSP metasurface and the incident light polarization configuration. (b) SEM image of the fabricated metasurface.

Numerical simulations were carried out by commercial full-wave simulation software CST Microwave Studio based on finite integration method to calculate the optical responses of the reflection phase tunable GSP metasurface. The simulation domain included one unit cell of the structures with period boundaries in x- and y-directions, and an open boundary was imposed in the z-direction. Plane wave was imposed to the unit cell along the z-direction with x-polarization (as shown in Fig. 1(a)). The permittivity of Au was described by the Drude model with plasma frequency $\omega_p = 1.37 \times 10^{16}$ rad/s and collision frequency $\gamma = 3 \times 4.08 \times 10^{13}$ s^{-1}.[27,28] The dispersion relationships of GST and SiO_2 were obtained by ellipsometer.

It is worth noting that besides stable amorphous and crystalline states, GST films in amorphous states can also be nucleated gradually to produce stable intermediate states by increasing heating temperature. The GST film in intermediate states consists of different proportions of amorphous and crystalline molecules, and the effective permittivities $\varepsilon_{\text{eff}}(\lambda)$ of the intermediate states can be determined by Lorentz–Lorenz relation[24,29]

$$\frac{\varepsilon_{\text{eff}}(\lambda)-1}{\varepsilon_{\text{eff}}(\lambda)+2} = m \times \frac{\varepsilon_{\text{c-GST}}(\lambda)-1}{\varepsilon_{\text{c-GST}}(\lambda)+2} + (1-m) \times \frac{\varepsilon_{\text{a-GST}}(\lambda)-1}{\varepsilon_{\text{a-GST}}(\lambda)+2}, \tag{1}$$

where m denotes the crystallization fraction of the GST film ranging from 0% to 100%, $\varepsilon_{\text{a-GST}}(\lambda)$ and $\varepsilon_{\text{c-GST}}(\lambda)$ represent the permittivities of GST in the amorphous and crystalline states, respectively.

The reflection spectra of the fabricated metasurface were measured by a Fourier transform infrared spectrometer (FTIR) with a KBr beam splitter. To be converted to the crystalline state gradually, a homemade in-situ heating device was combined with the FTIR. During the experiment, the heating temperature keeps increasing. When the temperature rises to 120°,

the reflection of the metasurface began to redshift. Therefore, 120° is selected as the starting point of GST phase transition. After that, the heating temperature was increased with the step of 10°. When the temperature rose above 200°, the reflection curve would not change with the increase of temperature, and in this way, the maximum temperature was determined as 200° during the measurement. In addition, in order to maintain the consistency of the experimental results, the heating time of each temperature was 2 minutes.

The comparison of reflection spectra obtained by experimental and simulated results is shown in Fig. 2. It can be observed that, within 120 THz–240 THz, the metasurface has only one response. The simulated results show that with the increase of GST crystallization fraction, the resonant frequency redshifts from 182 THz to 150 THz gradually. Accordingly, a similar redshift phenomenon can also be observed with the increase of heating temperature in the experimental results. In addition, the reflection of the metasurface also changes with the redshift of the resonant frequency. With the increase of GST crystallization fraction, the reflection decreases from 0.3 at 182 THz to near 0 at 150 THz. The corresponding reflection in the experimental results when GST is fully crystallized is less than 0.1. The simulated results agree well with the experimental data.

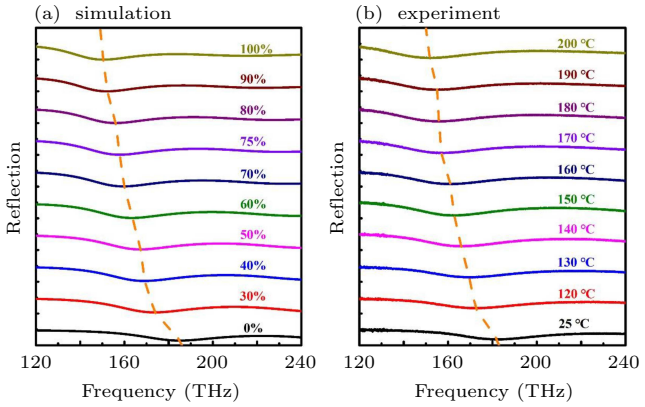


Fig. 2. The experimental and simulated reflection spectra of the metasurface. (a) Simulated reflection spectra with the increase of crystallization fraction of GST film. (b) Experimental reflection spectra with the increase of heating temperature.

The reflection phase was still obtained with the help of the FTIR. The metasurface was illuminated with a broadband infrared light source linearly polarized at a 45°-tilt angle with respect to the grating structure. The reflected signal intensity was measured after an analyzer with a deflection angle θ. Combined with the numerical fitting method, the spectra of the reflection phase with frequencies at various temperatures can be obtained (see supporting information). Figures 3(a) and 3(b) show the experimental results of reflection phase spectra at room temperature (RT), 150°, 200°, and the modulation effect of the reflection phase, namely the difference between the reflection phase at RT (amorphous GST) and at 200° (crystallized GST). The experimental results are compared with the simulated results, as shown in Figs. 3(c) and 3(d).

It can be intuitively observed from Fig. 3(b) that within the range of 150 THz–182 THz, significant reflection phase modulation has occurred, and the reflection phase difference $\Delta\varphi$ is greater than 200°.

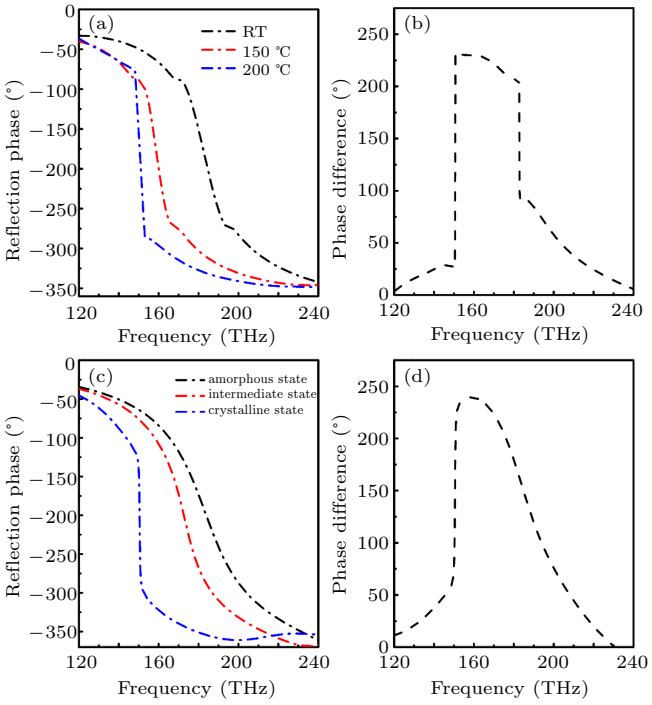


Fig. 3. The experimental and simulated reflection phase modulation effect of the tunable GSP metasurface. (a) The measured variation spectra of reflection phase with frequency under room temperature (black dashed line), 150° (red dashed line), and 200° (blue dashed line). (b) The measured reflection phase difference between amorphous GST and crystallized GST. (c) The simulated variation spectra of reflection phase with frequency when GST is in the amorphous state (black dashed line), 50%-intermediate state (red dashed line), and crystallized state (blue dashed line). (d) The simulated reflection phase difference between amorphous GST and crystallized GST.

Combined with the change of reflection and reflection phase, the modulation effects of the reflection phase tunable GSP metasurface are further analyzed. Figure 4 shows the spectra of reflection with the temperature at frequencies of 160 THz, 170 THz, 180 THz, and the corresponding reflection phase modulation effects.

It can be seen from Fig. 4 that, with the phase transition of GST, different reflection modulation effects occur at different frequencies. At 160 THz, the reflection phase difference $\Delta\varphi$ is more than 230° , but the modulation depth[30] of reflection is up to 82%. At 170 THz, a distinct change of reflection with temperature can still be observed, and the modulation depth is 55%. But the situation improves significantly at 180 THz, when the reflection phase difference remains above 200°, while the modulation depth of reflection decreases to 16%, and the reflection remains around 0.4, basically unchanged with temperature. This indicates that the loss of the whole metasurface is reduced and the work efficiency is significantly improved.

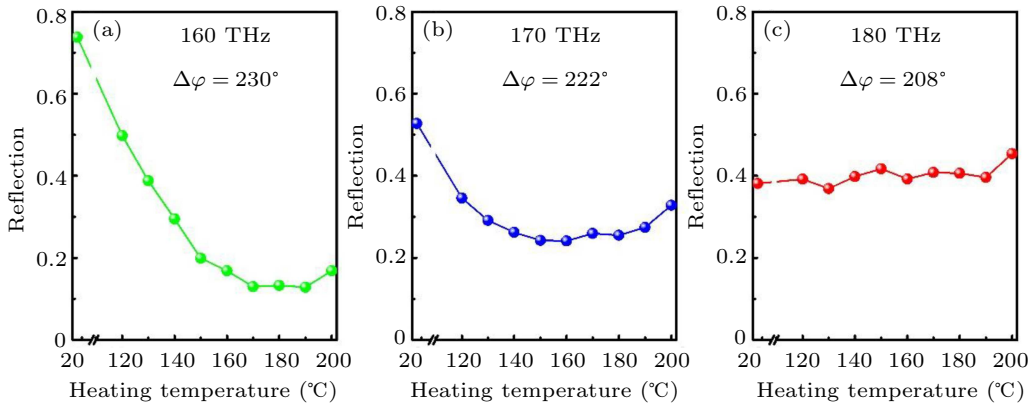


Fig. 4. Modulation effects of the reflection amplitude and phase at various frequencies of the tunable GSP metasurface. Panels (a), (b), and (c) represent the variation spectra of reflection with temperature and the corresponding reflection phase modulation effects at 160 THz, 170 THz, and 180 THz, respectively.

In order to further study the reflection phase modulation mechanism, the CMT is introduced, in which the GSP metasurface is described by a one-port single-mode resonator model. According to the CMT, the complex reflection coefficient r of such model is[26,31]

$$r = -1 + \frac{2\Gamma_r}{-i(\omega - \omega_0) + \Gamma_a + \Gamma_r}, \tag{2}$$

where Γ_r and Γ_a denote the loss caused by absorption within the resonator and the loss resulting from radiation to the far field. ω_0 represents the resonant circular frequency of the metasurface. For the one-port single-mode resonator model, the relative amplitudes of Γ_r and Γ_a determine the functionality of the GSP metasurface.[16] When $\Gamma_r > \Gamma_a$, the intrinsic absorption is weak and the resonator is overcoupling, the reflection phase $\Delta\varphi$ can cover a full 360° variation. On the contrary, in the $\Gamma_r < \Gamma_a$ region, the resonator transitions to undercoupling state, where the variation of $\Delta\varphi$ is less than 180° across the resonance. When $\Gamma_r = \Gamma_a$, the absorption of this model at its resonant frequency is $A = 1 - |r|^2 = 1$, which behaves as a perfect absorber.[32,33] With the increase of GST crystallization fraction, the relative amplitudes of Γ_r and Γ_a will change, which will cause the transition of the GSP metasurface working states.

According to Fig. 3(c) and combined with Eq. (1), the value of radiation loss Γ_r and intrinsic loss Γ_a at different GST crystallization fractions can be calculated, as shown in Fig. 5(a). It can be observed that with the increase of GST crystallization fraction, radiation loss Γ_r gradually decreases, and intrinsic loss Γ_a gradually increases. When GST is completely transformed into the crystallized state, $\Gamma_r = \Gamma_a$, and the GSP metasurface passes from the overcoupling state to the critical coupling state. In the process of GST crystallization, most of the GSP metasurface is in the overcoupling state with a large phase variation range, so a dramatic reflection phase modulation effect can be realized. The insert in Fig. 5(a) shows the magnetic field distribution in the cross section of the structure at the resonance of amorphous GST, which is a typical GSP mode resonance.[34] The evolution process of the working states of the GSP metasurface can be seen more intuitively by Smith curves, which show traces of r on the complex plane as frequency varies from 0 to ∞. Figure 5(b) displays the Smith curves of the GSP metasurface with three GST crystallization states, which are amorphous state, 50% crystalline state, and fully crystalline state, respectively. When GST is in the amorphous state, $\Gamma_r > \Gamma_a$, $\Delta\varphi$ approaches to 360° since the Smith curve covers four quadrants. In the case of a fully crystalline state, the Smith curve passes through the origin, which proves the transition from an overcoupling state to a critical coupling state.

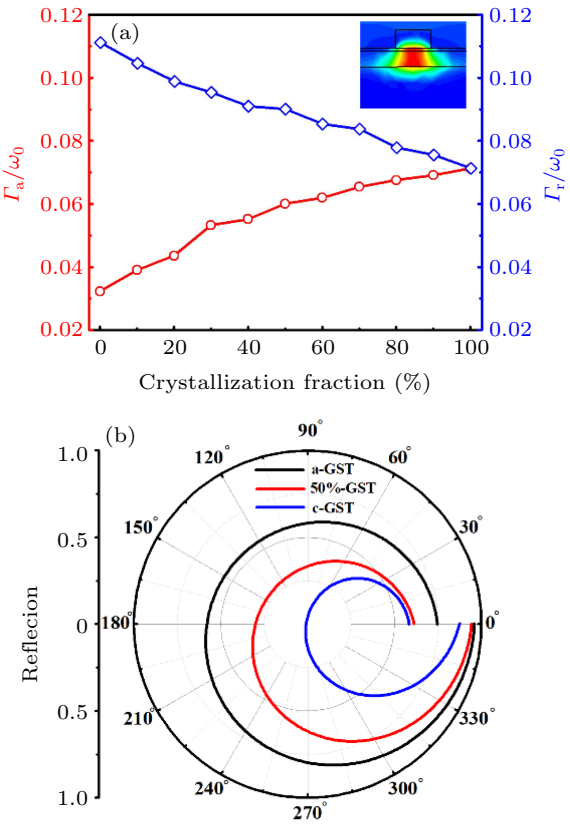


Fig. 5. (a) Spectra of Γ_r and Γ_a with GST crystallization fraction (inset: the magnetic field distribution in the cross section of the structure at the resonance of amorphous GST). (b) The Smith curves of the reflection coefficients with three GST crystallization states.

3. Conclusion and perspectives

In conclusion, a reflection phase tunable GSP metasurface in the near-infrared range has been proposed in this letter. This structure achieves a significant reflection phase modulation while realizing a stable reflection. Through the precise control of the thickness of GST dielectric layer and metal grating structure sizes, the dynamic continuous modulation effect with reflection phase greater than 200° of the GSP metasurface in the 150 THz–182 THz range was finally realized experimentally. Especially in the frequency of 180 THz, the reflection is larger than 0.38 and the modulation depth is only 16%, which greatly reduces the loss of the metasurface and shows a more practical application prospect of the structure in wavefront shaping. In addition, the CMT is introduced to study the modulation mechanism, which proves that the phase transition of GST mainly changes the working mode of the GSP metasurface, realizing the transition from the overcoupling state to the critical coupling state. In the case of the overcoupling state, the metasurface has the ability to continuously change the reflection phase by 360° , which is the basis for the realization of large angle reflection phase tunability.

References

[1] Kildishev A V, Boltasseva A and Shalaev V M 2013 *Science* **339** 1232009
[2] Chen H T, Taylor A J and Yu N 2016 *Rep. Prog. Phys.* **79** 076401
[3] Su V C, Chu C H, Sun G and Tsai D 2018 *Opt. Express* **26** 13148
[4] Yin X, Steinle T, Huang L, Taubner T, Wuttig M, Zentgraf T and Giessen H 2017 *Light Sci. Appl.* **6** e17016
[5] Huang L, Chen X, Muhlenbernd H, Li G, Bai B, Tan Q, Jin G, Zentgraf T and Zhang S 2012 *Nano Lett.* **12** 5750
[6] Pors A and Bozhevolnyi S I 2013 *Opt. Express* **21** 27438
[7] Ni X, Ishii S, Kildishev A V and Shalaev V 2013 *Light Sci. Appl.* **2** e72
[8] Aieta F, Genevet P, Kats M A, Yu N, Blanchard R, Gaburro Z and Capasso F 2012 *Nano Lett.* **12** 4932
[9] Pors A, Nielsen M G, Eriksen R L and Bozhevolnyi S 2013 *Nano Lett.* **13** 829
[10] Wang S, Wu P C, Su V C, Lai Y, Chu C, Chen J, Lu S, Chen J, Xu B, Kuan C, Li T, Zhu S and Tsai D 2017 *Nat. Commun.* **8** 187
[11] Chen W T, Yang K Y, Wang C M, Huang Y, Sun G, Chiang I, Liao C, Hsu W, Lin X, Sun S, Zhou L, Liu A and Tsai D 2014 *Nano Lett.* **14** 225
[12] Deng Z L, Deng J, Zhuang X, Wang S, Li K, Wang Y, Chi Y, Ye X, Xu J, Wang G, Zhao R, Wang X, Cao Y, Cheng X, Li G and Li X 2018 *Nano Lett.* **18** 2885
[13] Huang Y W, Chen W T, Tsai W Y, Wu P, Wang C, Sun G and Tsai D 2015 *Nano Lett.* **15** 3122
[14] Zheng G, Muhlenbernd H, Kenney M, Li G, Zentgraf T and Zhang S 2015 *Nat. Nanotechnol.* **10** 308
[15] Ding F, Yang Y, Deshpande R A and Bozhevolnyi S I 2018 *Nanophotonics* **7** 1129
[16] Qu C, Ma S, Hao J, Qiu M, Li X, Xiao S, Miao Z, Dai N, He Q, Sun S and Zhou L 2015 *Phys. Rev. Lett.* **115** 235503
[17] Berry M V 1987 *J. Mod. Opt.* **34** 1401
[18] Park J, Kang J H, Kim S J, Liu X and Brongersma M L 2017 *Nano Lett.* **17** 407
[19] Kafaie Shirmanesh G, Sokhoyan R, Pala R A and Atwater H 2018 *Nano Lett.* **18** 2957
[20] Huang Y W, Lee H W, Sokhoyan R, Pala R A, Thyagarajan K, Han S, Tsai D and Atwater H 2016 *Nano Lett.* **16** 5319
[21] Sherrott M C, Hon P W C, Fountaine K T, Garcia J C, Ponti S M, Brar V W, Sweatlock L A and Atwater H A 2017 *Nano Lett.* **17** 3027
[22] Miao Z, Wu Q, Li X, He Q, Ding K, An Z, Zhang Y and Zhou L 2015 *Phys. Rev. X* **5** 041027
[23] Pitchappa P, Kumar A, Prakash S, Jani H, Venkatesan T and Singh R 2019 *Adv. Mater.* **31** e1808157
[24] Qu Y, Li Q, Du K, Cai L, Lu J and Qiu M 2017 *Laser Photonics Rev.* **11** 1700091
[25] Fu Q, Zhang F, Fan Y, Dong J, Cai W, Zhu W, Chen S and Yang R 2017 *Appl. Phys. Lett.* **110** 221905
[26] Wonjoo S, Zheng W and Shanhui F 2004 *IEEE J. Quantum Electron.* **40** 1511
[27] Zhang S, Fan W J, Malloy K J, Brueck S, Panoiu N and Osgood R M 2006 *J. Opt. Soc. Am. B-Opt. Phys.* **23** 434
[28] Linden S, Enkrich C, Wegener M, Zhou J, Koschny T and Soukoulis C 2004 *Science* **306** 1351
[29] Aspnes D E 1982 *Am. J. Phys.* **50** 704
[30] Li C, Zhu W, Liu Z, Yan S, Pan R, Du S, Li J and Gu C 2018 *Appl. Phys. Lett.* **113** 231103
[31] Fan S H, Suh W and Joannopoulos J D 2003 *J. Opt. Soc. Am. A-Opt. Image Sci. Vis.* **20** 569
[32] Celanovic I, Perreault D and Kassakian J 2005 *Phys. Rev. B* **72** 075127
[33] Hao J M, Wang J, Liu X, Padilla W J, Zhou L and Qiu M 2010 *Appl. Phys. Lett.* **96** 251104
[34] Jung J, Søndergaard T and Bozhevolnyi S I 2009 *Phys. Rev. B* **79** 035401